

# The effect of ocean mixed layer depth on climate in slab ocean aquaplanet experiments

Aaron Donohoe · Dargan M. W. Frierson ·  
David S. Battisti

Received: 21 April 2013 / Accepted: 10 June 2013 / Published online: 28 June 2013  
© Springer-Verlag Berlin Heidelberg 2013

**Abstract** The effect of ocean mixed layer depth on climate is explored in a suite of slab ocean aquaplanet simulations with different mixed layer depths ranging from a globally uniform value of 50–2.4 m. In addition to the expected increase in the amplitude of the seasonal cycle in temperature with decreasing ocean mixed layer depth, the simulated climates differ in several less intuitive ways including fundamental changes in the annual mean climate. The phase of seasonal cycle in temperature differs non-monotonically with increasing ocean mixed layer depth, reaching a maximum in the 12 m slab depth simulation. This result is a consequence of the change in the source of the seasonal heating of the atmosphere across the suite of simulations. In the shallow ocean runs, the seasonal heating of the atmosphere is dominated by the surface energy fluxes whereas the seasonal heating is dominated by direct shortwave absorption within the atmospheric column in the deep ocean runs. The surface fluxes are increasingly lagged with respect to the insolation as the ocean deepens which accounts for the increase in phase lag from the shallow to mid-depth runs. The direct shortwave absorption is in phase with insolation, and thus the total heating comes back in phase with the insolation as the ocean deepens more and the direct shortwave absorption dominates the seasonal heating of the atmosphere. The intertropical convergence zone follows the seasonally varying insolation

and maximum sea surface temperatures into the summer hemisphere in the shallow ocean runs whereas it stays fairly close to the equator in the deep ocean runs. As a consequence, the tropical precipitation and region of high planetary albedo is spread more broadly across the low latitudes in the shallow runs, resulting in an apparent expansion of the tropics relative to the deep ocean runs. As a result, the global and annual mean planetary albedo is substantially (20 %) higher in the shallow ocean simulations which results in a colder (7C) global and annual mean surface temperature. The increased tropical planetary albedo in the shallow ocean simulations also results in a decreased equator-to-pole gradient in absorbed shortwave radiation and drives a severely reduced ( $\approx 50$  %) meridional energy transport relative to the deep ocean runs. As a result, the atmospheric eddies are weakened and shifted poleward (away from the high albedo tropics) and the eddy driven jet is also reduced and shifted poleward by  $15^\circ$  relative to the deep ocean run.

**Keywords** Seasonal cycle · Aquaplanet · Expansion of tropics

## 1 Introduction

The seasonal cycle of temperature in the extratropics is driven by seasonal variations in insolation that are comparable in magnitude to the annual mean insolation. The majority of the seasonal variations in insolation are absorbed in the ocean Fasullo and Trenberth (2008a, b), which has a much larger heat capacity than the overlying atmosphere. This energy never enters the atmospheric column to drive seasonal variations in atmospheric temperature and circulation. The heat capacity of the ocean

---

A. Donohoe (✉)  
Department of Earth, Atmospheric and Planetary Sciences,  
Room Number 54-918, 77 Massachusetts Avenue,  
Cambridge, MA 02139-4307, USA  
e-mail: thedhoe@mit.edu

D. M. W. Frierson · D. S. Battisti  
Department of Atmospheric Sciences, University of Washington,  
Seattle, WA, USA

plays a fundamental role in setting both the magnitude and phasing of the seasonal cycle in the atmosphere. The Earth's climate would be fundamentally different if the ocean's heat capacity was not substantially larger than that of the atmosphere.

In a forced system with a heat capacity and negative feedbacks (damping), the phase lag of the response increases with increasing heat capacity, reaching quadrature phase with the forcing in the limit of very large heat capacity (Schneider 1996). Therefore, in the extratropical climate system—where the insolation is the forcing and the Planck feedback and dynamic energy fluxes are the dominant negative feedbacks—one would expect that the phase lag of temperature with respect to insolation would increase with increasing ocean heat capacity. We will demonstrate that this expectation is not realized in a set of experiments with an idealized climate model; the phase lag of atmospheric temperature is a non-monotonic function of ocean heat capacity. We argue that increasing ocean heat capacity moves the system from a regime in which the seasonal heating of the atmosphere is dominated by the energy fluxes from the surface (ocean) to the atmosphere to a regime where the heating is dominated by the sun heating the atmosphere directly via shortwave absorption in the atmospheric column. In the latter regime, the surface and atmospheric energy budgets are partially decoupled and the atmospheric heating is nearly in phase with the insolation resulting in a small phase lag of the seasonal temperature response. Recently, Donohoe and Battisti (2013) demonstrated that the seasonal heating of the atmosphere in the observations is dominated by direct shortwave absorption in the atmospheric column as opposed to surface energy fluxes, which is akin to the large ocean heat capacity regime discussed above.

The heat capacity of the climate system does not contribute to the annual mean energy budget in the theory of energy balance models (North 1975) because there is no heat storage in equilibrium. However, the magnitude of the seasonal cycle can impact the annual mean energy budget through the rectification of non-linearities and/or the covariance of processes acting over the seasonal cycle (i.e. the correlation between seasonal anomalies in insolation and albedo). Therefore, the ocean heat capacity may impact the annual mean climate. Indeed, we demonstrate here that the ocean heat capacity has a large impact on the modeled climate system in the annual mean including the global mean temperature, the global energy budget, the extent of the tropics, the meridional energy transport, and the location and intensity of the surface westerlies.

Slab ocean models are widely used to assess the equilibrium climate sensitivity in global climate models (Danabasoglu and Gent 2009) because the system comes to equilibrium rapidly as compared to the full-depth ocean

model. Slab ocean models are also widely used in idealized simulations (Kang et al. 2008; Rose and Ferreira 2013) to model the response of the climate system to prescribed anomalies in ocean heat transport. The sensitivity of climate to mixed layer depth in these simulations is often neglected.

In this study, we analyze the effect of slab ocean depth on climate (temperature, precipitation, winds, and energy fluxes) in a suite of aquaplanet slab ocean experiments, each with a different, globally uniform ocean mixed layer depth. This paper is organized as follows. In Sect. 2, we introduce the models and observational data sets we will compare the models to. We then analyze the amplitude and phase of the seasonal cycle of atmospheric temperature and interpret these results in terms of the source of the seasonal heating of the atmosphere (Sect. 3). In Sect. 4, we analyze the seasonal migration of the inter-tropical convergence zone (ITCZ) in the slab-ocean aquaplanet simulations and its impact on the tropical precipitation. We also demonstrate in this section that the seasonal migration of the ITCZ causes a large residual contribution to the global and annual average planetary albedo and, hence, the global energy budget and global mean temperature. Lastly, in Sect. 5, we demonstrate that the amplitude of the seasonal cycle also modifies the meridional heat transport in the climate system by way of modifying the meridional structure of planetary albedo. As a consequence, both the magnitude and location of the jets, including the surface westerlies, change as the amplitude of the seasonal cycle changes. A summary and discussion follows in Sect. 6.

## 2 Data and methods

We will analyze the effect of ocean heat capacity on climate in a suite of slab-ocean aquaplanet simulations with different ocean mixed layer depths. Here we describe the model runs used. The analysis of the model output will then be compared to observations to put the results in context. We also describe the observational data sources in this section.

### 2.1 Slab-ocean aquaplanet simulations

We couple an atmospheric general circulation model to a uniform constant depth slab ocean that covers the entire globe—hereafter an aquaplanet. We perform five experiments with prescribed ocean depths of 2.4, 6, 12, 24, and 50 m. The heat capacity of the 2.4 m slab ocean is equivalent to that of the atmosphere while the heat capacity in the 50 m run is more than 20 times that of the atmosphere. There is no Q flux to the ocean; the ocean does not transport energy. Sea ice is prohibited from forming in the

model, even if the sea-surface temperature is below the freezing point of sea water. The atmospheric model is the Geophysical Fluid Dynamics Lab Atmospheric Model version 2.1 (Delworth et al. 2006) featuring a finite volume dynamical core (Lin 2004) with a horizontal resolution of approximately  $2^\circ$  latitude,  $2.5^\circ$  longitude and 24 vertical levels. The model is forced by seasonally varying solar insolation with zero eccentricity and  $23.439^\circ$  obliquity. The model is run for twenty years and the model climatology is taken from the last five years of the integrations; these choices ensure the model is spun up and the seasonal cycle is adequately sampled.

The atmospheric energy budget is

$$\frac{dE}{dt} = SWABS + SHF - OLR - \nabla \cdot (\mathbf{UMSE}), \quad (1)$$

where  $E$  is the column integral of sensible and latent heat ( $C_p T + Lq$ ),  $OLR$  is the outgoing longwave radiation,  $MSE$  is the moist static energy ( $C_p T + Lq + gZ$ ), and the term on the right represents the atmospheric energy flux convergence integrated over the column of the atmosphere.  $SWABS$  is the shortwave absorption within the atmospheric column, and represents the sun directly heating the atmosphere:

$$SWABS = SW_{\downarrow TOA} - SW_{\uparrow TOA} + SW_{\uparrow SURF} - SW_{\downarrow SURF}. \quad (2)$$

$SHF$  is the net (turbulent plus longwave radiation) exchange of energy between the surface and the atmosphere:

$$SHF = SENS_{\uparrow SURF} + LH_{\uparrow SURF} + LW_{\uparrow SURF} - LW_{\downarrow SURF}, \quad (3)$$

where  $SENS$  is the sensible energy flux and  $LH$  is the latent energy flux, both defined as positive upwards to the atmosphere. We note that  $SHF$  does not include solar fluxes because the surface solar fluxes are an exchange of energy between the surface and the sun and the solar impact on the atmospheric budget is accounted for in  $SWABS$ . See Donohoe and Battisti (2013) for further discussion.

We calculate  $SWABS$  and  $SHF$  from Eqs. 2 and 3 respectively using the model output of the fluxes at the top of the atmosphere (TOA) and the surface.  $\frac{dE}{dt}$ , hereafter the storage, is calculated from the finite difference of the monthly column integrated temperature and specific humidity. The energy transport convergence is calculated as the residual of Eq. 1.

## 2.2 Observational data

We use the ERA-Interim Reanalysis climatological (1979–2010) atmospheric temperature data to define the amplitude and phase of the observed atmospheric temperature. The radiative fluxes used are from the corrected long

term climatologies (Fasullo and Trenberth 2008b) of the Clouds and Earth's Radiant Energy System (CERES) experiment (Wielicki et al. 1996). The atmospheric energy flux convergences are from Donohoe and Battisti (2013) and are derived from ERA-Interim Reanalysis using the advective form of the equations.  $SWABS$  is assessed directly from the climatological averaged CERES data including the (AVG) surface shortwave fluxes.  $SHF$  is calculated as a residual from Eq. 1.

## 3 The amplitude and phase of the seasonal cycle of atmospheric temperature and the source of atmospheric heating

The seasonal amplitude of temperature, defined as the amplitude of the annual harmonic, in the slab-ocean aquaplanet simulations is shown in the left panel of Fig. 1. As expected, the seasonal amplitude decreases with increasing mixed layer depth at both the surface (solid lines) and in the mid-troposphere (dashed line). In the shallow mixed layer depth runs, the seasonal cycle of temperature is larger at the surface than it is in the mid-troposphere. In contrast, the seasonal amplitude of temperature is largest in the mid-troposphere for the deep mixed layer depth runs. The observed amplitude of the seasonal cycle above the Southern Ocean (between  $30^\circ S$  and  $65^\circ S$ —upper right panel of Fig. 1) resembles that of the 50 m run, with a small amplitude and amplified seasonal cycle aloft. Poleward of  $65^\circ S$  the influence of the Antarctic continent can be seen with a larger and surface amplified seasonal amplitude of temperature. The seasonal amplitude in the Northern extratropics is comparable in magnitude to the 12 m run and shows the surface amplification seen in the shallow mixed runs, reflecting the large and surface amplified seasonal cycle over the land masses.

The phase lag of the tropospheric averaged (below 250 hPa) temperature relative to the insolation varies non-monotonically with mixed layer depth (bottom panel of Fig. 1); the phase lag in the high-latitudes (poleward of  $50^\circ$ ) increases as the mixed-layer depth increases from 2.4 to 12 m but then decreases as the mixed layer depth increases further from 12 to 50 m. This behavior is not expected from a system with a single heat capacity dictated by the ocean mixed-layer depth. The observed seasonal cycle of temperature has a substantially smaller phase lag than any of the aquaplanet simulations (lower right panel of Fig. 1). The vertical structure of the phase of the seasonal cycle in temperature (Fig. 2) shows that the phase is nearly vertically uniform in the shallow mixed layer depth experiments, suggesting that the entire column responds in unison to seasonal variations in insolation. In contrast, in the deep mixed layer runs, the temperature aloft leads that

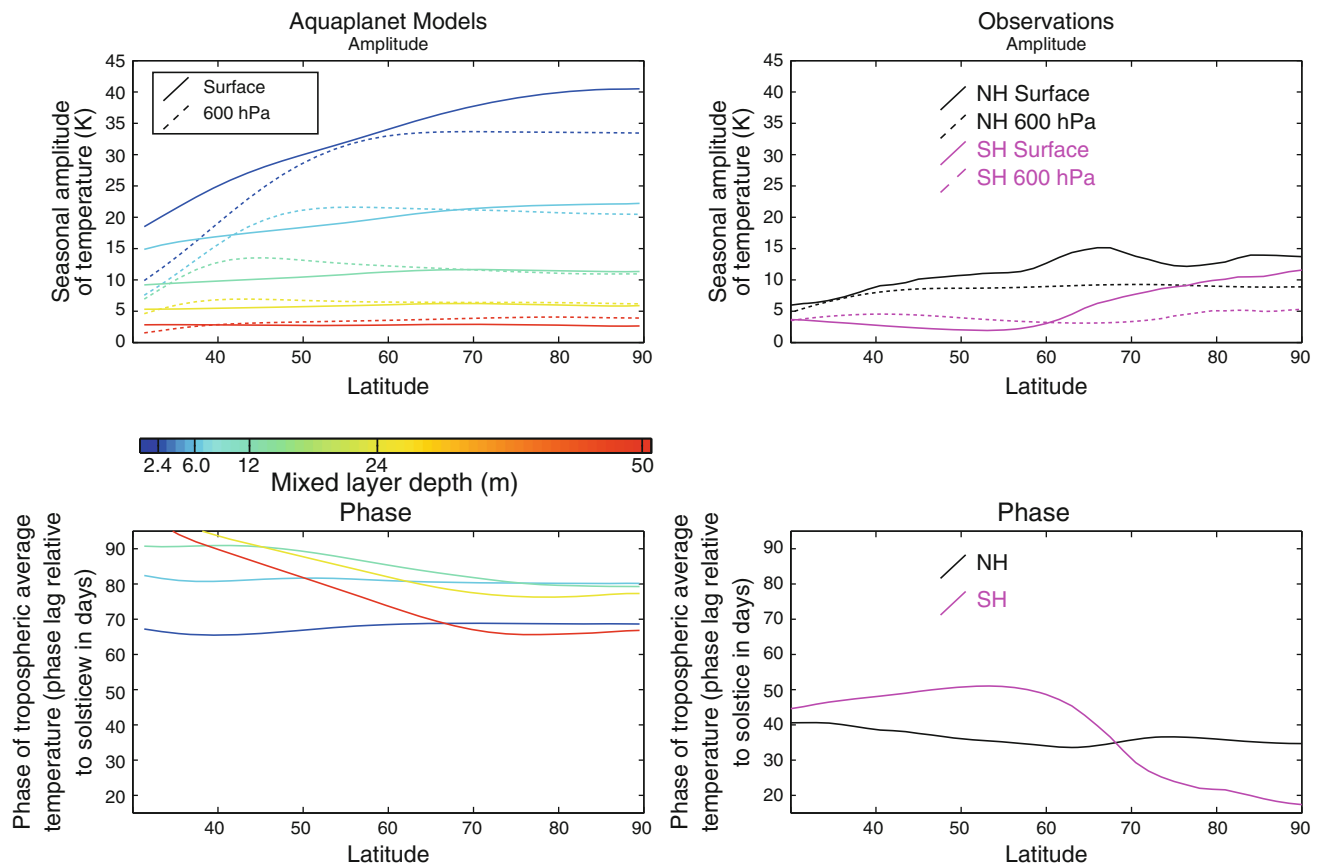


**Fig. 1** (Top) The seasonal amplitude of atmospheric temperature at the surface (*solid lines*) and at 600 hPa (*dashed lines*) in the slab-ocean aquaplanet simulations (*left panel*) and observations (*right panel*). The different ocean mixed layer depths are indicated by the colorbar below the plot. (Bottom) Phase lag of seasonal cycle of

tropospheric averaged (below 250 hPa) temperature with respect to insolation in the slab-ocean aquaplanet simulations (*left*) and observations (*right*). The phase lag is expressed in days past the summer solstice

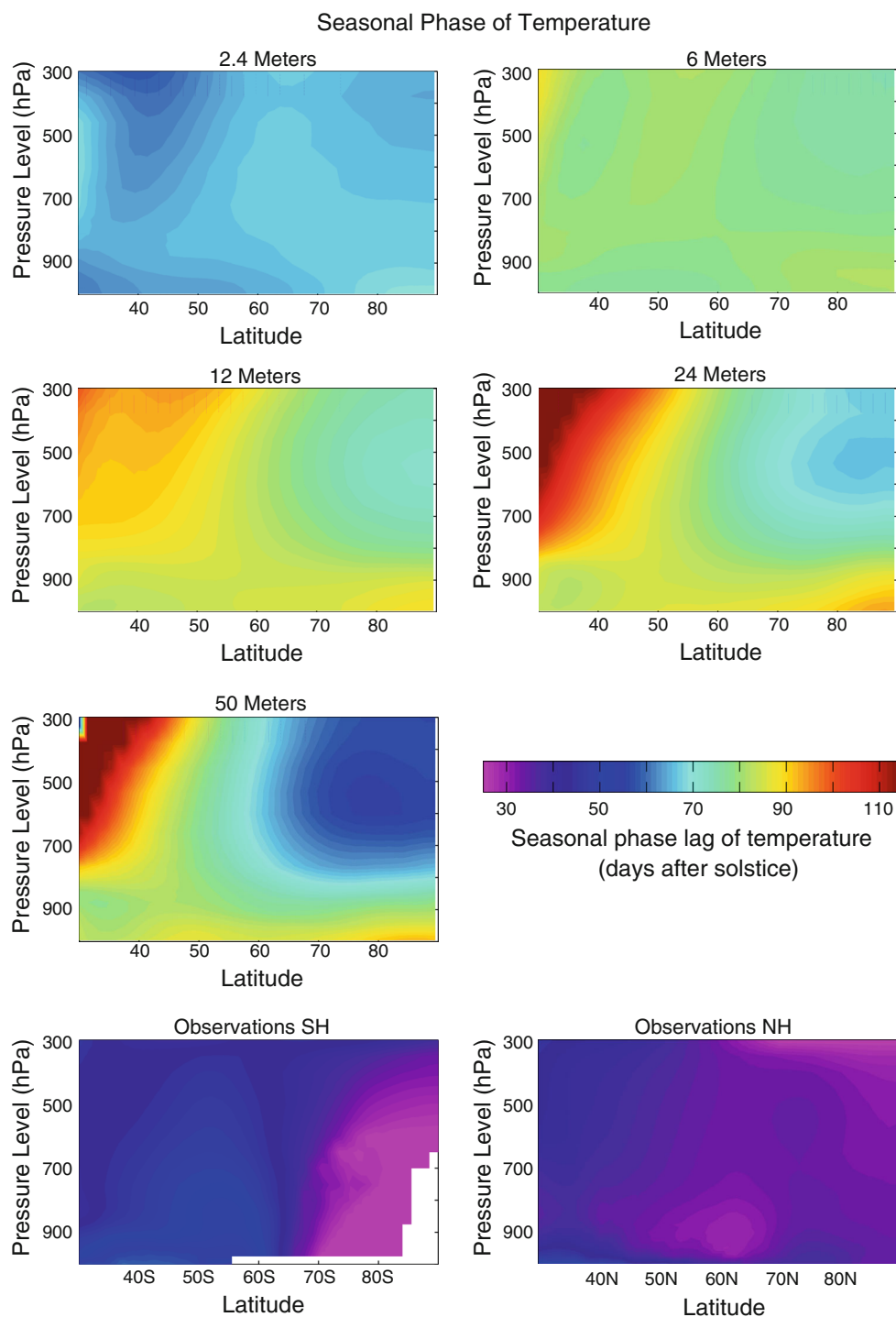
at the surface by of order one month in the high latitudes.<sup>1</sup> The observed seasonal cycle of temperature has a smaller phase lag than the aquaplanet simulations at all levels. The observed temperature aloft leads that at the surface (akin to the deep mixed layer depth runs) over the Southern Ocean whereas the phase is nearly vertical invariant (akin to the shallow mixed layer depth runs) throughout the Northern extratropics and over Antarctica.

We argue that the effect of ocean mixed layer depth on the amplitude, phase, and vertical structure of the seasonal cycle in temperature can be understood by analyzing the source of the seasonal heating of the atmosphere. Specifically, the seasonal heating of the atmosphere is dominated by the upward energy fluxes from the ocean to the

<sup>1</sup> We note that the seasonal cycle of temperature in the deep runs is delayed aloft in the vicinity of 40°. This phase lag is a consequence of reduced eddy energy flux divergence during the warm season that is driven by extratropical atmospheric heating which leads to a reduced meridional temperature gradient aloft during the late summer. This acts as a phase delayed source of heating in the subtropical troposphere which is driven non-locally

atmosphere (SHF) in the shallow mixed layer experiments whereas it is dominated by direct absorption of shortwave radiation (*SWABS*) in the deep mixed-layer depth experiments. The time series of the seasonal heating (annual mean removed) of the atmosphere by *SWABS*, *SHF* and their sum (total heating) averaged poleward of 40°N is shown in Fig. 3. *SWABS* has a seasonal amplitude of order  $50 \text{ W m}^{-2}$ , is nearly in phase with the insolation and varies very little with mixed layer depth. This result is consistent with water vapor and ozone in the atmosphere absorbing approximately 20 % of the insolation (Chou and Lee 1996) during all seasons. The increased amplitude and phase lag of *SWABS* in the 2.4 m runs is a consequence of the moistening of the extratropical hemisphere during the late summer, resulting in seasonal variations in the fraction of insolation absorbed in the column that peak in late summer. We also note that the seasonal cycle of *SWABS* in the observations are well replicated in the models suggesting that the basic state shortwave absorptivity is well captured in the aquaplanet model.

**Fig. 2** Meridional-height cross sections of the phase of the seasonal cycle of atmospheric temperature in each of the slab-ocean aquaplanet simulations (*upper panels*) and the observations (*lower panels*). Values are expressed as the phase lag relative to the insolation in days



In contrast to the nearly mixed-layer depth invariant *SWABS*, the seasonal cycle of *SHF* decreases markedly with increasing mixed-layer depth while the phase lag concurrently increases with increased mixed layer depth. In the limit of zero surface heat capacity, we would expect the upward *SHF* to match the net shortwave radiation at the surface because, there can be no storage

in the surface. In the 2.4 m run, the seasonal amplitude of the *SHF* is  $75\text{W m}^{-2}$  and is 62 % of the amplitude of the net shortwave radiation at the surface. The *SHF* lags the surface solar radiation by 29 days. Although the heat capacity of the ocean is non-negligible in the 2.4 m run, the majority of the surface shortwave radiation gets fluxed upward to the atmospheric column with a small



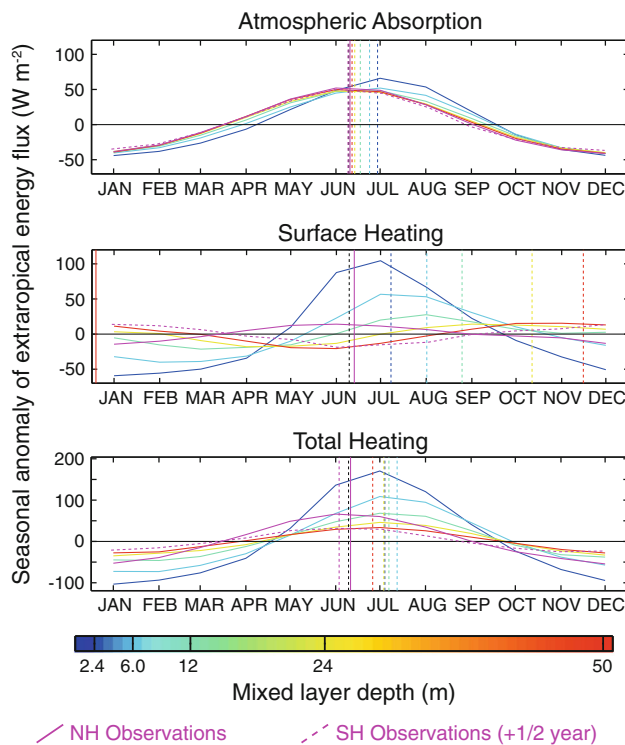


**Fig. 3** Time series of atmospheric heating averaged over the Northern Extratropics defined as poleward of  $40^{\circ}\text{N}$ . The total atmospheric heating (*bottom panel*) is decomposed into contributions from solar absorption in the atmospheric column ( $SWABS$ —*top*) and surface energy fluxes ( $SHF$ —*middle panel*). The annual mean value of each contribution has been subtracted from the time series. The different ocean mixed layer depths are indicated in the *colorbar* at the *bottom* and the observations in the Northern and Southern hemisphere are shown by the *solid* and *dashed purple lines* respectively. The  $SH$  curve has been shifted by half a year. The *vertical dashed lines* represent the phase of the seasonal cycle and the *vertical dashed black line* is the summer solstice

time lag.<sup>2</sup> In contrast, in the 50 m run, the entirety of the seasonal variations in surface shortwave radiation (not shown) are stored in the ocean mixed-layer; the seasonal amplitude of energy storage in the extratropical ocean exceeds the seasonal amplitude of net shortwave radiation at the surface (by 20 %) as the atmosphere fluxes energy to the ocean via downward a  $SHF$  during the warm season. The latter flux is made possible by the fact that the atmosphere is being heated directly by  $SWABS$

<sup>2</sup> We note that, the seasonal amplitude of extratropical shortwave radiation absorbed at the surface is in phase with the insolation but has 57 % of the seasonal amplitude of the insolation ( $125 \text{ W m}^{-2}$  as compared to  $220 \text{ W m}^{-2}$ ) which represents the shortwave opacity of the atmosphere times the surface co-albedo (0.92). Thus, in the limit of zero surface heat capacity we would expect that approximately 57 % of the seasonal insolation to enter the atmospheric column via  $SHF$  as compared to the 20 % of insolation absorbed directly in the atmospheric column ( $SWABS$ ). In this case, there is an approximately 3:1 heating ratio of  $SHF$ : $SWABS$ , similar to the observed annual mean ratio (Donohoe and Battisti 2013).

in the summer and losing energy via the interaction with the ocean surface. This also explains why the seasonal cycle of temperature is amplified aloft in the deep mixed layer depth runs (upper left panel of Fig. 1) since the distribution of  $SWABS$  is nearly invariant throughout the troposphere (Donohoe and Battisti 2013) but the loss of energy to the ocean is confined to the boundary layer.

The suite of aquaplanet mixed-layer experiments span two different regimes of seasonal energy input into the atmosphere; the seasonal heating of the atmosphere is dominated by the  $SHF$  in the shallow mixed layer runs while the seasonal heating of the atmosphere is dominated by  $SWABS$  in the deep mixed layer runs (Fig. 3). The transition between the two regimes occurs for the 6 and 12 m runs where both  $SWABS$  and  $SHF$  contribute to the seasonal heating of the atmosphere. The phase lag of  $SHF$  increases with increasing mixed layer depth as a consequence of the sea surface temperatures lagging the insolation more as the thermal inertia of the system increases.

The phase of the total heating varies non-monotonically with mixed layer depth and can be understood in terms of the transition between a regime where seasonal heating is dominated by  $SHF$  to one where  $SWABS$  dominates the seasonal heating of the atmosphere. If the atmosphere was transparent to shortwave radiation ( $SWABS = 0$ ) then the phase lag of atmospheric temperature would increase monotonically with increasing ocean mixed layer depth along with the phase of  $SHF$ . Indeed, as the ocean mixed layer depth increases from 2.4 to 6 m, the total seasonal heating of the atmosphere becomes more phase lagged, reflecting the contribution  $SHF$  (Fig. 3, bottom panel). However, the amplitude of  $SHF$  also decreases with increasing mixed layer depth and the seasonal heating of the atmosphere becomes increasingly dominated by  $SWABS$ ;  $SWABS$  and  $SHF$  have nearly identical seasonal amplitudes in the 6m run and the seasonal amplitude of  $SWABS$  exceeds that of  $SHF$  by a factor of three in the 24 m run. Because  $SWABS$  is nearly in phase with the insolation (and  $SHF$  lags the insolation), the phase lag of total atmospheric heating decreases as the mixed layer depth increases from 6 to 50 m and the seasonal heating becomes dominated by  $SWABS$ . In the 50 m run, the seasonal flow of energy between the atmosphere and the surface has completely reversed relative to the 2.4 m run (and the annual mean): the atmosphere is heated directly by the sun during the warm season and subsequently fluxes energy downward to the ocean resulting in an amplified and phase leading seasonal cycle aloft relative to the surface (Figs. 1, 2 respectively).

The relative roles of  $SHF$  and  $SWABS$  in the seasonal heating of the atmosphere in the suite of aquaplanet mixed layer depth experiments is best demonstrated by the seasonal amplitude of the energy fluxes averaged over the

extratropics (defined as poleward of 38°) shown in Fig. 4. The seasonal amplitude is defined as the amplitude of the Fourier harmonic in phase with the total atmospheric heating (*SHF* plus *SWABS*) and has been normalized by the amplitude of the total heating in each experiment to emphasize the relative magnitude of each of the terms. This definition of amplitude takes into account both amplitude and phase with positive amplitudes amplifying the seasonal cycle in temperature and negative amplitudes damping the seasonal cycle. As discussed above, *SWABS* and *SHF* make comparable contributions to the seasonal heating of the atmosphere in the 2.4 and 6 m runs (the red and blue diamonds have similar positive magnitudes) while the heating of the atmosphere is dominated by *SWABS* in the deeper mixed layer. In the 24 and 50 m runs, *SWABS* is the sole source of seasonal atmospheric heating as the *SHF*s are out of phase with the heating and, thus, damp the

seasonal cycle of atmospheric temperature. We note that, the latter situation also occurs in the observed Southern Hemisphere (top panel of Fig. 4) where the seasonal flow of energy is from the sun heating the atmosphere during the summer and the atmosphere subsequently losing energy to the surface (Donohoe and Battisti 2013). In the observed Northern Hemisphere, *SHF* contributes to the seasonal heating of the atmosphere due to a contribution from the land domain where the vast majority of downwelling shortwave radiation at the surface is fluxed upward to the atmosphere with a small time lag as a consequence of the small heat capacity of the surface. As the extratropical atmosphere is heated seasonally, energy is lost to *OLR*, atmospheric energy flux divergence, and storage in the atmospheric column (see Eq. 1) with all three terms making nearly equal magnitude contributions. The extratropical atmosphere is moister during the summer in the shallow mixed layer depth experiments compared to the deeper simulations and to Nature. Hence, atmospheric energy storage has a relatively larger damping contribution to the seasonal cycle in the shallow mixed layer runs compared to the deeper mixed layer simulations and Nature.

The seasonal phasing of atmospheric temperature is a direct consequence of the amplitude and phasing of seasonal heating discussed above. The bottom panel of Fig. 4 shows the phase of all the energy flux terms averaged over the extratropics in the aquaplanet simulations and observations. The phase of the total heating of the atmosphere (red–blue diamonds) varies non-monotonically as a function of mixed layer depth because the seasonal heating transitions from being dominated by *SHF* (shallow runs) to being dominated by *SWABS* (deep runs). As a result, the phase of the tropospheric averaged temperature also varies non-monotonically with mixed layer depth: the temperature lags the total atmospheric heating by 43 days in the ensemble of experiments and observations. This phase lag of the temperature relative to the total heating is consistent with a forced system with negative net (linear) feedbacks where the heat capacity times the angular frequency of the forcing is approximately equal to the sum of the feedback parameters (Donohoe 2011). The seasonal energy storage within the atmospheric column is comparable to the sum of the losses by radiative (*OLR*) and dynamic ( $\nabla \cdot (UMSE)$ ) processes (top panel of Fig. 4). Thus the temperature tendency leads the atmospheric heating by  $\approx 45^\circ$  of phase and the feedbacks lag the heating by the same amount. The essential point is that, provided the dynamic and radiative feedbacks are nearly climate state invariant, the phase of atmospheric heating will dictate the phase of the temperature and energetic response as can be seen by the corresponding changes in the phase of total atmospheric heating (blue–red diamonds in the bottom panel of Fig. 4) and temperature (black diamonds) across the suite of

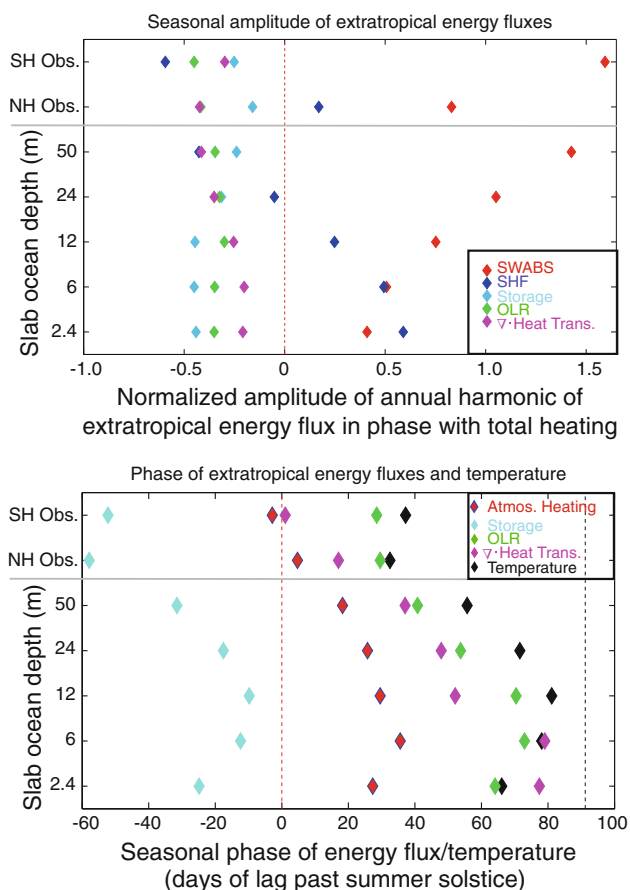


**Fig. 4** (Top panel) The normalized seasonal amplitude of energy fluxes to the extratropics, defined as the amplitude of the annual harmonic in phase with the total atmospheric heating (*SWABS* + *SHF*). The amplitude is normalized by the amplitude of the total heating to demonstrate the relative amplitude of the terms in the different mixed layer depth experiments. (Bottom panel) The phase of the various energy flux terms in the extratropics. The temperature is the atmospheric column integrated temperature. The red and black dashed vertical lines represent the solstice and equinox respectively

aquaplanet simulations. Finally, we note that the atmospheric heating in the observations occurs earlier in the calendar year than in all the aquaplanet simulations—even than the 2.4 m mixed layer depth simulation. As a consequence, the phase lag of atmospheric temperature relative to the insolation is smaller in the observations than in the aquaplanet simulations at all heights and latitudes (Fig. 2). This result suggests that even the small quantity of land mass in the Southern Hemisphere is essential to setting the phase of atmospheric temperature over the whole domain and will be discussed further in Sect. 6.

#### 4 The seasonal migration of the ITCZ and its impact on precipitation and global mean temperature

The zonally averaged ITCZ migrates seasonally into the summer hemisphere where the maximum sea surface temperatures (SST) and atmospheric heating are found (Chiang and Friedman 2012; Frierson et al. 2013). The seasonal migration of the ITCZ decreases as the depth of the slab ocean increases in the aquaplanet simulations as more of the seasonal variations in extratropical insolation

are stored in the ocean, resulting in smaller seasonal variability of the SSTs and energy fluxes to the atmosphere. We argue that the magnitude of the seasonal migration of the ITCZ off the equator critically controls the annual mean meridional extent of the tropics as measured by the meridional structure of cloud cover, precipitation, and planetary albedo. As a consequence, the magnitude of the seasonal migration of the ITCZ also controls the global mean energy balance and surface temperature.

##### 4.1 The seasonal migration of the ITCZ and the meridional extent of the tropics

The top panel of Fig. 5 shows the meridional overturning streamfunction in the atmosphere averaged over the three months when the ITCZ is located farthest north alongside the precipitation (blue lines) and planetary albedo (orange lines). In the 50 m mixed layer depth run, the maximum precipitation remains within  $3^\circ$  of the equator during all seasons and is co-located with the SST maximum (not shown). The ascending branch of the Hadley circulation is confined to within  $10^\circ$  of the equator and the subsidence occurs between  $10^\circ$  and  $25^\circ$  during all seasons. In contrast,

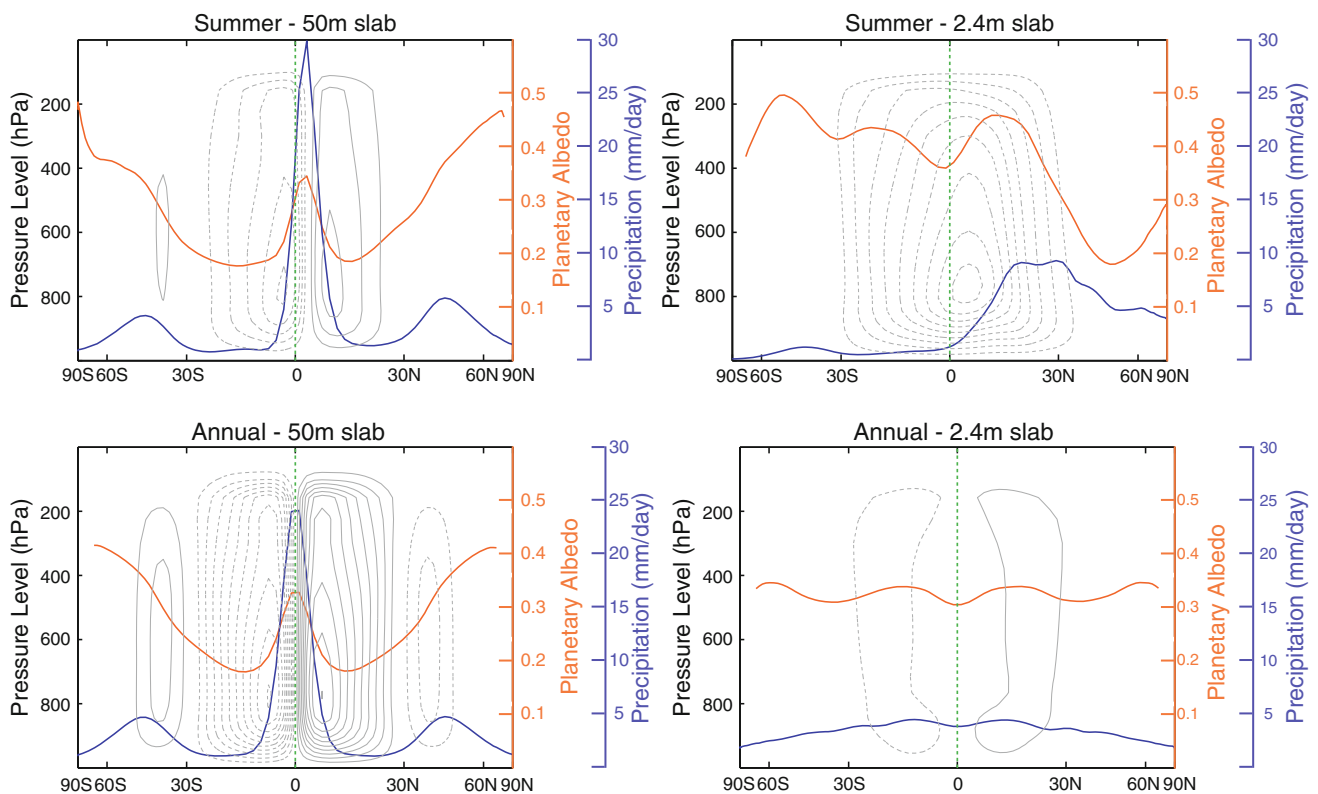


**Fig. 5** (Top panels) Boreal summer and (bottom panels) annual mean mass overturning streamfunction, precipitation, and planetary albedo for the (left panels) 50 m and (right panels) 2.4 m slab ocean simulations. The mass overturning streamfunction is shown in gray contours with solid lines denoting clockwise rotation and dashed line

denoting counter-clockwise rotation. The contour interval is 50 Sv ( $10^9 \text{kg s}^{-1}$  for the top panels and 20 Sv for the bottom panels). The zonal mean planetary albedo is the orange line and the precipitation is the blue line (with scales given by the orange and blues axes to the right respectively)



in the 2.4 m slab ocean depth run, the precipitation maximum and ascending branch of the Hadley cell extends to approximately  $30^\circ$  during the seasonal extrema (upper right panel of Fig. 5). As the ITCZ migrates off the equator in the shallow mixed layer run, a large amplitude asymmetry develops between the winter and summer Hadley cells (Lindzen and Hou 1988) with the summer cell nearly disappearing. As a result the precipitation maximum occurs within the winter cell. Compared to the 50m run, the ascending motion and precipitation are spread over a broad latitudinal extent (Donohoe et al. 2013). There is strong subsidence in the winter hemisphere leading to an inversion and stratus clouds that extend from the equator to  $30^\circ$  (not shown). Stratus is less persistent over the same subtropical region in the deeper mixed layer runs because the subsidence strength is reduced and the SST remains higher in the winter due to the larger thermal inertia of the ocean.

The magnitude of the seasonal migration of the ITCZ and the concomitant precipitation, and clouds have a profound impact on the annual mean climate of the tropics and subtropics. In the deep mixed layer depth runs, the annual mean climate is similar to that of seasonal extrema and features a strong and narrowly confined Hadley cell (lower left panel of Fig. 5—note that the contour interval of the streamfunction has been reduced relative to the upper panels) with ascending motion and convective precipitation within  $10^\circ$  of the equator and subsidence and dry conditions from  $10^\circ$  to  $30^\circ$ . Similarly, the meridional structure of the zonally averaged planetary albedo is very similar to the seasonal extrema, with high values over the precipitating regions and low values over the extensive and dry subtropics. In contrast, the annual mean climate in the shallow mixed layer depth run is fundamentally different from that of the seasonal extrema. The strong ascent that occurs during the local summer is nearly, but not exactly, balanced by subsidence during the local winter. As a consequence, the annual mean mass overturning circulation is extremely weak and meridionally expansive in the 2.4 m run as compared to the 50 m run (c.f. the gray contours in the lower right and lower left panels of Fig. 5). The annual mean precipitation is spread nearly uniformly across the tropics for two reasons: the precipitation follows the seasonally migrating ITCZ and thus covers the whole region equatorward of  $30^\circ$ , and the ascending regions and precipitation extend over a broader region in the shallow mixed layer depth runs due to the amplitude asymmetry between the winter and summer branches of the Hadley cell. The planetary albedo is also nearly uniform across the tropics as a result of the convective precipitation that covers a broad region in the summer hemisphere accompanied by an equally extensive region of stratus clouds in the winter hemisphere (see top right panel of Fig. 5). Overall, the tropics expand poleward in the shallow mixed

layer depth runs (relative to the deep run) as measured from common metrics of the tropical extent including the annual mean precipitation minus evaporation, the outgoing longwave radiation, and the mass overturning streamfunction (Johanson and Fu 2009).

#### 4.2 Planetary albedo and the globally and annually averaged temperature

The meridional structure of the annual mean planetary albedo is dramatically different in the shallow and deep ocean mixed layer depth experiments. In the deep ocean runs, there is a well defined contrast between the high albedo tropics and low albedo subtropics. In contrast, the shallow ocean runs feature a meridionally broad high albedo tropical region. The meridional extent of the high planetary albedo tropical region expands poleward as the depth of the ocean mixed layer decreases (right panel of Fig. 6). The extratropical planetary albedo is highest for the deeper mixed layer depth runs and is a consequence of a seasonally persistent mid-latitude baroclinic zone and storm track in the deep runs. In contrast the mid-latitude baroclinic zone and storm track only exists in the winter in the shallow ocean runs; in the shallow ocean runs, the extratropical storm track vanishes along with the baroclinicity during the summer months (the maximum SSTs are found between  $40^\circ$  and  $50^\circ$ ). As a result, there are fewer clouds and lower extratropical planetary albedo in the annual mean in the shallow runs. The differences in tropical and extratropical planetary albedo across the suite of ocean mixed layer depth simulations partially but far from completely compensate for one another in the global average with the tropical response dominating the global mean behavior. The global mean planetary albedo for each simulation is shown by the thick horizontal lines on the right and left axes of the right panel of Fig. 6. The global mean planetary albedo increases with decreasing mixed layer depth and varies by 0.05 across the suite of simulations which corresponds to a global mean top of the atmosphere (TOA) shortwave radiation difference of  $15\text{W m}^{-2}$ . We note that, the seasonal covariance of planetary albedo and insolation makes a negligible contribution to the annual and global mean planetary albedo in all runs (i.e. the seasonal insolation weighted annual mean albedo is comparable to the annual mean albedo in all regions).

The zonal and annual mean SST differs greatly across the suite of slab ocean aquaplanet simulations (left panel of Fig. 6) and are a consequence of the differences in global mean planetary albedo. The global average SST is  $7\text{C}$  higher in the 50 m ocean slab depth run than in the 2.4 m slab depth run which is significantly colder than the other runs. Overall, the differences in global mean surface temperature across the suite of simulations follow the global

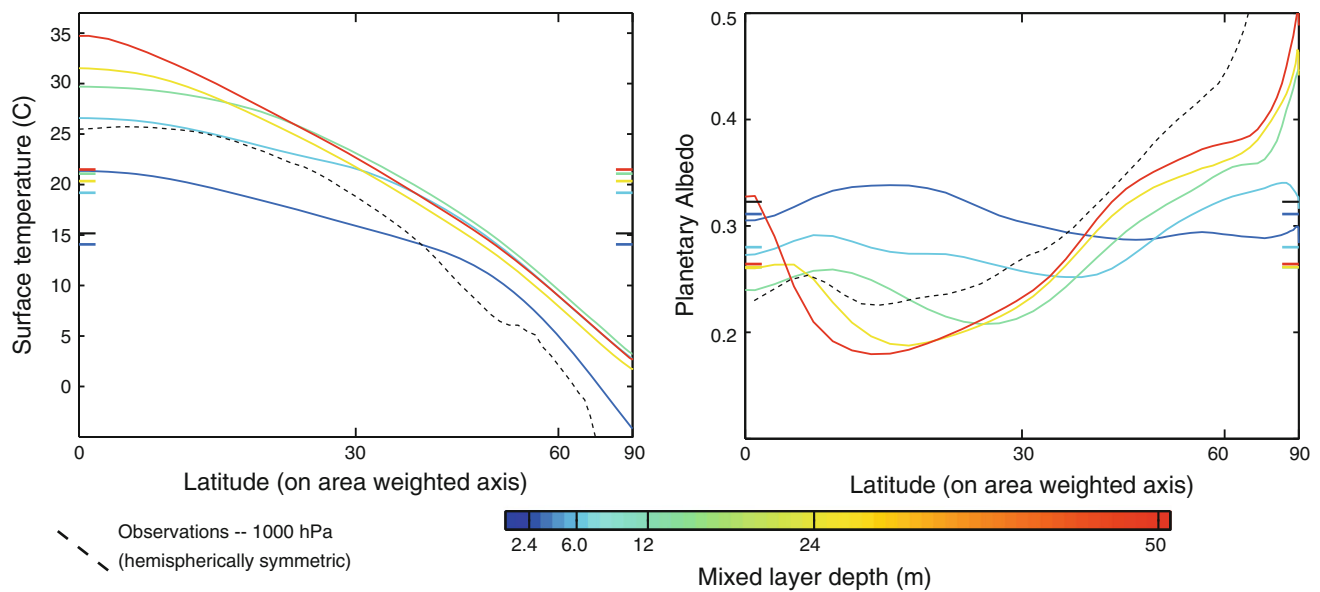


**Fig. 6** (Left panel) Zonal and annual mean surface temperature and (right panel) planetary albedo. Each of the colors is a different aquaplanet slab ocean simulation with slab depth given by the color

bar on the bottom. The dashed black line is the observations averaged over both hemispheres. The thick horizontal lines on the left and right hand side of plot is the global mean value for each run

mean absorbed shortwave radiation ( $ASR = S[1 - \alpha_p]$ ) with a  $2 \text{ W m}^{-2}$  increase in ASR corresponding to an approximately 1 degree C increase in global mean temperature. The low-latitude SSTs (equatorward of  $30^\circ$ ) increase monotonically with increasing mixed layer depth concurrent with the decrease in local planetary albedo. In contrast, the differences in extratropical SST across the suite of experiments do not follow the differences in local ASR. For example, the extratropics of the 2.4 m run are the coldest of the entire ensemble despite the fact that the local planetary is the lowest amongst all the ensemble members. This result suggests that the global mean energy balance is communicated to all regions of the globe by way of the (atmospheric) meridional energy transport, regardless of the local radiative differences. We further pursue the changes in meridional energy transport in the next section.

## 5 Meridional energy transport and jet location

In the previous section, we demonstrated that the meridional structure of planetary albedo differs drastically across the suite of slab ocean aquaplanet simulations. The equator-to-pole gradient of planetary albedo plays a fundamental role in determining the meridional heat transport in the climate system (Stone 1978; Enderton and Marshall 2009). The mid-latitude heat transport is primarily accomplished by eddies in the atmosphere (Czaja and Marshall 2006) and the eddies affect the jet location and the surface winds (Edmon et al. 1980). Therefore, any change in the magnitude and/or spatial structure of

meridional heat transport is expected to be accompanied by a shift in the jet. In this section, we demonstrate that there are first order changes in the annual mean meridional heat transport and zonal winds across the suite of slab ocean aquaplanet simulations.

### 5.1 Meridional energy transport

The annually averaged meridional energy transport in the slab ocean aquaplanet simulations is shown in Fig. 7. We note that, there is no ocean energy transport in these simulations which allows the atmospheric energy transport to be calculated from spatially integrating the net radiative imbalance at the TOA from pole to pole. The contribution of the mean overturning circulation (MOC—i.e. the Hadley and Ferrel cells) to the energy transport is calculated from the monthly mean meridional velocity, temperature, specific humidity and geopotential field using the advective form of the energy flux equation as in Donohoe and Battisti (2013). The eddy contribution is calculated as the total energy transport minus the MOC energy transport.<sup>3</sup> The peak in energy transport is almost 2 PW higher in the deep ocean runs (5.4 PW in the 50 m simulation) as compared to the shallow ocean runs. The meridional structure of the energy transport is more meridionally peaked for the deep runs as compared to the flatter structure seen for the shallow runs.

<sup>3</sup> The stationary eddies make a negligible contribution to the total energy transport. The stationary eddy energy transport is included in the eddy energy transport term for completeness.

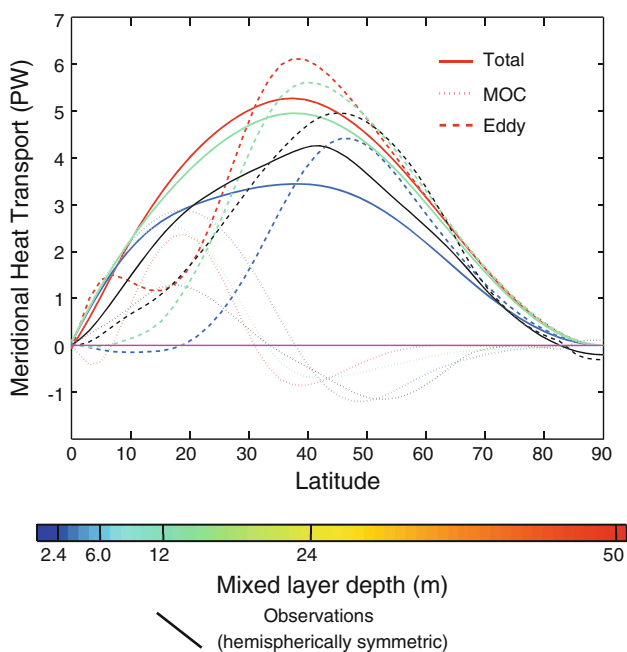


**Fig. 7** (Solid lines) Meridional energy transport partitioned into mean meridional overturning circulation (MOC—vertically dashed line) and eddy contribution (horizontal dashed lines). The 50, 12, and 2.4 m slab ocean depth simulations are shown, with colors given by the legend at the bottom of the figure

The partitioning of the energy transport into MOC and eddy components shows several anticipated features (Fig. 7). In the low latitudes, the energy transport is dominated by a poleward energy transport in the thermally direct Hadley cell<sup>4</sup> and the eddies make a negligible contribution (with the exception of the deep tropics of the 50 m run). The Hadley cell energy transport extends farther poleward in the shallow runs due to the expansion of the tropics that was previously noted. In the mid-latitudes, the eddies dominate the total energy transport and the MOC energy transport is equatorward in the thermally indirect Ferrel cell. The peak equatorward energy transport in the Ferrel cell is co-located with the eddy energy transport maximum in all runs which is consistent with the Ferrel cell being driven by the eddies.

The reduced meridional energy transport in the shallow mixed layer depth runs (relative to deep runs) is accompanied by weaker eddy energy transport in the mid-latitudes (c.f. the blue and red dashed lines in Fig. 7). From the perspective of the TOA radiation budget, the increased subtropical planetary albedo in the shallow run results in a smaller magnitude net radiative surplus and demands

<sup>4</sup> The equatorward MOC energy transport in the deep tropics of the 50 m run is a consequence of the moist static energy decreasing with height in the boundary layer due to a very moist and warm boundary layer. This results in the Hadley cell transporting energy in the same direction as the meridional flow at the surface.

weaker eddy energy flux divergence and therefore weaker mid-latitude eddies; the weaker eddies result from a reduced meridional gradient in shortwave heating between the subtropics and the extratropics. From the perspective of the local dynamics, the mid-latitude baroclinity in the shallow runs is severely reduced during the summer as the maximum SSTs are found around 40°. As a result, the mid-latitude storm track essentially disappears (along with the baroclinity) during the summer in the shallow runs whereas the storm track is nearly seasonally invariant in the deep runs. The seasonal variations in storm track intensity and location results in weaker eddies in the annual mean in the shallow runs as compared to the deep runs. We note that, the eddy energy flux maximum is shifted 10° poleward in the 2.4 m run as compared to the 50 m run (peaking at 47° as compared to 37°). This shift is a consequence of the differences in the meridional extent of the Hadley cell energy transport and differences in the total heat transport demanded by the TOA radiation budget as a consequence of the changes in subtropical planetary albedo associated with the seasonal migration of the Hadley cell (see Fig. 6). The ramifications of the reduced and poleward shifted eddies in the shallow run will be further discussed in Sect. 5b.

The maximum meridional energy transport between the tropics and the extratropics ( $MHT_{MAX}$ ) is equal to the net radiative deficit at the TOA spatially integrated over the extratropics (Trenberth and Caron 2001). As such, it can be thought of as the ASR anomaly relative to the global mean integrated over the extratropics ( $ASR^*$ ) minus the outgoing longwave radiation anomaly integrated over the same region ( $OLR^*$ —see Donohoe and Battisti 2012, for a discussion):

$$MHT_{MAX} = ASR^* - OLR^* \tag{4}$$

$ASR^*$  is a consequence of the meridional gradient in incident radiation and the meridional gradient of planetary albedo. The latter was shown in Sect. 4b to differ substantially with ocean mixed layer depth with a larger meridional gradient in planetary albedo for the deep ocean runs (c.f. the red and blue lines in the right panel of Fig. 6). One would therefore expect the deep ocean runs, with a stronger meridional gradient in planetary albedo, to have enhanced meridional energy transport ( $MHT_{MAX}$ ) provided that the spatial gradients in absorbed radiation ( $ASR^*$ ) are not completely balanced by local changes in emitted radiation ( $OLR^*$ ). In physical terms, when the extratropics have a higher planetary albedo than the tropics, the equator-to-pole contrast of energy input into the climate system is enhanced ( $ASR^*$  increases) and the system must balance the enhanced gradient in absorbed insolation by fluxing more energy from the tropics to the extratropics (increasing  $MHT_{MAX}$ ) or by coming to equilibrium with a larger equator to pole temperature gradient resulting in a larger OLR gradient by the Planck feedback (increasing

**Table 1** The peak poleward energy transport ( $MHT_{MAX}$ ) and its partitioning into the extratropical deficit in absorbed shortwave ( $ASR^*$ ) and emitted longwave radiation ( $OLR^*$ ) in the slab ocean aquaplanet simulations

Mixed layer depth (m)	$MHT_{MAX}$ (PW)	$ASR^*$ (PW)	$OLR^*$ (PW)
50	5.3	8.3	3.0
24	5.0	8.0	3.0
12	4.8	7.5	2.7
6	4.3	6.2	1.9
2.4	3.4	5.0	1.6

$OLR^*$ ).  $ASR^*$  increases from 5.0 PW in the 2.4 m depth run to 8.3 PW in the 50 m depth run (Table 1) and the majority of the changes in  $ASR^*$  are balanced by enhanced energy transport into the extratropics ( $MHT_{MAX}$ ) while changes in  $OLR^*$  play a secondary role in balancing differences in  $ASR^*$  across the suite of simulations. This result suggests that differences in the equator-to-pole gradient in absorbed shortwave radiation are primarily balanced by changes in the dynamic energy transport and secondarily by local radiative adjustment (by way of the Planck feedback). This result is consistent with the findings of Donohoe and Battisti (2012) and Enderton and Marshall (2009) who found that changes in the meridional structure of planetary albedo are mainly balanced by changes in the total meridional energy transport in the climate system.

5.2 Zonal jets and surface winds

In the previous section, we found that deepening the ocean mixed layer resulted in an increase and equatorward shift of the annual mean eddy energy flux as a consequence of the changes in tropical planetary albedo and the associated total energy transport change demanded by the equator-to-pole scale energy budget at the TOA. Here, we examine the relationship between the eddy energy flux and the zonal jet and surface winds across the suite of slab ocean aquaplanet simulations. Figure 8 shows the cross sections of the annually and zonally averaged zonal winds for the 50 m run (red) and the 2.4 m run (blue). The upper tropospheric jet in the 50 m run is stronger in magnitude, and shifted equatorward by approximately 15° latitude relative to its counterpart in the 2.4 m run. The jet shift extends all the way to the surface where the winds are more than twice the magnitude and shifted 15° equatorward in the 50 m run as compared to the 2.4 m run.

The intensity and location of the surface winds across the ensemble of slab ocean aquaplanet simulations are readily understood given the changes in the eddy energy fluxes that were discussed in Sect. 5a. The acceleration of the zonal winds is equal to the divergence of the Eliassen-Palm flux ( $\mathbf{F}$ —Eliassen and Palm 1961). At the surface,

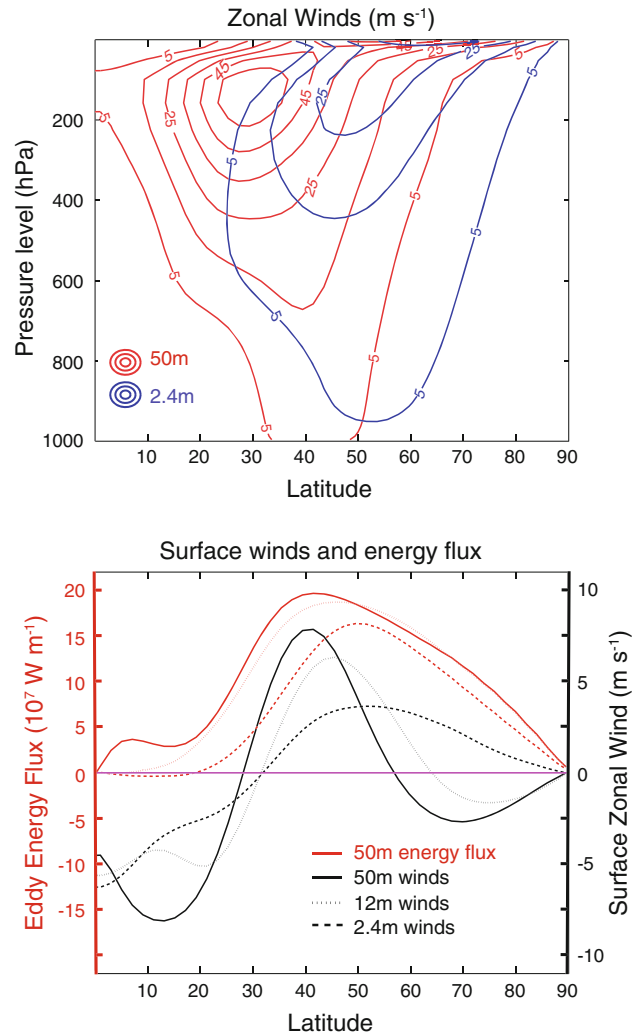


**Fig. 8** (Top panel) The annual and zonal mean zonal wind cross section for the 50 m deep slab ocean simulation (red contours) and the 2.4 m run (blue contours). The contour interval is 10ms<sup>-1</sup> and only positive contours are shown. The contour (Bottom panel) Zonally averaged eddy energy flux (red lines in 10<sup>7</sup> W m<sup>-1</sup> with scale to the left) and surface zonal wind (black lines in m s<sup>-1</sup> with scale to the right) in the slab ocean aquaplanet simulations. The 50 m run is shown with the solid line. The 12 m run is shown with the vertical dashed line and the 2.4 m run is shown with the horizontal dashed line

$\nabla \cdot \mathbf{F}$  (and  $\mathbf{F}$ ) is dominated by the vertical component (Andrews and McIntyre 1976) which is proportional to the eddy energy flux. Neglecting the horizontal (eddy momentum flux) component of the Eliassen-Palm flux, the acceleration of the zonal wind at the surface is:

$$\frac{\partial U_{SURF}}{\partial t} \approx f \frac{\partial}{\partial p} \left( \frac{V^* \left[ \theta^* + \frac{L}{C_p} q^* \right]}{\sigma_0} \right) \tag{5}$$

(Stone and Salustri 1984) where  $V$  is the meridional velocity,  $\theta$  is the potential temperature,  $q$  is the specific humidity,  $*$  denotes the eddy component and  $\square$  is the zonal



and time average of the eddy covariance.  $\sigma_0$  is the basic state static stability,  $f$  is the Coriolis parameter and  $p$  is pressure. Conceptually, the meridional eddy energy flux (moist static energy) accelerates the zonal flow by acting as a form drag on isentropic surfaces (Vallis 2006). We note that, this derivation assumes that the basic state stratification is substantially larger than the spatial variability of the static stability, and thus, the impact of the spatially varying static stability on zonal jet is neglected in this theory and the discussion below. The argument of the pressure derivative is the eddy (moist static) energy flux. Provided that there is no energy flux at the surface, and the eddy energy fluxes vary smoothly in the vertical, peaking somewhere in the troposphere, the zonal acceleration of the winds in the lower troposphere will be proportional to the vertically integrated meridional energy flux. The dominant momentum balance at the surface is between the eddy acceleration of the zonal winds and the frictional damping at the surface. Provided that the frictional damping is proportional to the surface winds, the surface winds should be proportional to and peak at the same location as the maximum in eddy energy flux.

The annual and zonal average eddy energy flux is co-plotted with the the surface winds for the suite of slab ocean aquaplanet simulations in the lower panel of Fig. 8. We note that the zonal average eddy energy flux that appears in Eq. 5 and Fig. 8 differs from the zonally integrated energy flux that is shown in Fig. 7 by the zonal circumference at each latitude. The latter contains a factor of the cosine of latitude and thus the zonally averaged eddy energy flux peaks poleward of the zonally integrated energy flux which is constrained by the spherical geometry of the Earth (Stone 1978). In all simulations, the maximum surface westerlies are co-located with the peak in the eddy energy flux (c.f. the red and black lines in the lower panel of Fig. 8). The maximum eddy energy flux in the 2.4 m depth run is located approximately  $15^\circ$  poleward of its counterpart in the 50 m run and the jet shifts meridional by approximately the same distance. The meridional structure and relative amplitudes of the surface westerlies across the suite of simulations also mimic the differences in the eddy energy flux. These results collectively suggest that Eq. 5 and the approximations discussed in the paragraph above are a reasonable, albeit simplistic representation of the system behavior. The location of the maximum surface winds respond to the vertically averaged eddy energy fluxes which themselves are constrained by the equator-to-pole scale radiative budget.

## 6 Summary and discussion

The amplitude of the seasonal cycle in temperature and energy fluxes increases with decreasing ocean mixed layer

depth in suite of slab ocean aquaplanet simulations. This expected behavior is accompanied by several less intuitive results including: (1) the phase of the seasonal cycle in temperature varies non-monotonically with ocean mixed layer depth (bottom left panel of Fig. 1), (2) the tropics are more meridionally expansive in the shallow depth runs (lower panel of Fig. 5), (3) the annual and global mean surface temperature is of order  $5\text{C}$  lower in the shallow runs as compared to the deep runs (left panel of Fig. 6), (4) the mid-latitude meridional energy transport is reduced by of order 50 % in the shallow runs (Fig. 7) and (5) the zonal winds shift poleward by more than  $10^\circ$  in the shallow mixed layer depth runs (Fig. 8). Below, we review the mechanisms responsible for these results and discuss the behavior of the observed climate system relative to the suite of aquaplanet mixed layer depth simulations.

The seasonal heating of the atmosphere can be decomposed into two contributions: the sun heating the surface and the surface subsequently fluxing energy to the atmosphere by turbulent and longwave energy fluxes (SHF), and the sun directly heating the atmosphere by shortwave absorption (SWABS) in the atmospheric column (Donohoe and Battisti 2013). The surface fluxes dominate the seasonal heating of the atmosphere in the shallow ocean runs while the entirety of the seasonal heating of the atmosphere is due to SWABS in the deeper ocean runs (Fig. 3). The surface contribution to the seasonal heating of the atmosphere has a larger phase lag relative to the insolation for the deeper runs, and this explains the initial increase in phase lag of atmospheric temperature as the mixed layer depth increase from 2.4 to 12 m. However, as the mixed layer depth increases beyond 12 m, the seasonal heating of the atmosphere becomes increasingly dominated by SWABS, which is in phase with the insolation, and the total heating of the atmosphere comes back into phase with the insolation. The phase of seasonal variations in temperature and energy fluxes across the suite of aquaplanet simulations and the observations are readily explained by the phase of atmospheric heating (bottom panel of Fig. 4).

The net seasonal heating of the observed climate system is dominated by SWABS in both hemispheres (purple lines in Fig. 3) with the exception of the mid-latitude continents (Donohoe and Battisti 2013). The observed phase lag of the atmospheric temperature relative to the insolation is smaller than even in the 2.4 m slab ocean simulations. We note that, the phase of the total atmospheric heating relative to the insolation in the observations is also smaller than that in the aquaplanet simulations and that the phase of atmospheric temperature is well predicted given the phase of the atmospheric heating (c.f. the red diamonds with the black diamonds in the lower panel of Fig. 4). The cause of the smaller phase lag between the insolation and the net atmospheric heating in the observations relative to the



aquaplanet simulations is unclear and we speculate on the possible causes below. One possibility is that, the presence of land with a near zero heat capacity over even a small subset of the domain sets the phase of atmospheric heating and temperature over the whole domain. Because the land surface has such a small heat capacity, seasonal variations in downwelling shortwave radiation are transferred to the overlying atmosphere with near zero-phase lag. This source of energy input into the atmosphere is communicated hemispherically by way of the atmospheric advection with a time scale of order one week (Donohoe 2011) and a fraction even ends up in the ocean mixed layer (Donohoe and Battisti 2013). Thus, the land surface serves as a large input of energy into the atmosphere with near zero phase lag and could set the phase of temperature over the entire globe. It is possible that even the small amount of land in the Southern Hemisphere sets the phase of seasonal variations in temperature above the Southern Ocean which also exhibits a pronounced phase lead of temperature relative to the aquaplanet simulations (Fig. 2). Other possible explanations for the discrepancy between the model and the observations include, the seasonal cycle of ocean circulation (e.g. the ocean energy flux convergence over this region), the seasonal shoaling of the thermocline, the role of sea-ice cover (sea-ice is prohibited from forming in the aquaplanet simulations), and an inadequate representation of the turbulent energy fluxes in the model.

In simple, linear, energy balance models, the heat capacity of the climate system has no effect on the annual mean climate since there is no energy storage in equilibrium. We have demonstrated that, the ocean mixed layer depth has a profound effect on the annual mean climate in a suite of aquaplanet simulation. The mixed layer depth's influence on the annual mean climate is a consequence of the seasonal seasonal migration of the ITCZ and its impact on planetary albedo and can be explained as follows. The enhanced seasonal cycle of SSTs and atmospheric energy fluxes in the shallow mixed layer experiments results in the ITCZ migrating farther off the equator seasonally (top panel Fig. 5). As the ITCZ moves off the equator, an asymmetry between the winter and summer Hadley cells develops resulting in a broad region of ascent and convective precipitation in the summer hemisphere and extensive stratus in the winter hemisphere. The time average of the seasonally migrating ITCZ in the shallow ocean runs is a very weak annual mean Hadley cell with precipitation and high planetary albedo broadly spread over the low-latitudes. This is a stark contrast to the deeper ocean runs where ascending branch of the Hadley cell is confined to within  $10^\circ$  of the equator (during all seasons) resulting in a small region of convective precipitation and high planetary albedo and a well defined dry and cloud free subtropical region. The Tropics expand and broaden in the

shallow mixed layer depth runs resulting in a high global mean planetary albedo. As a result, the annual mean temperature decreases in the shallow runs (Fig. 6). The enhanced planetary albedo in the shallow runs is confined to the tropics which results in a decreased equator-to-pole gradient of absorbed shortwave radiation and reduced meridional energy transport (Fig. 7). The peak in eddy energy transport is both reduced and shifted poleward in the shallow ocean runs which results in a poleward shift and weakening of the eddy-driven jet (Fig. 8). This sequence of causality emphasizes that clouds play a central role in determining both the global mean and spatial pattern of ASR and, therefore, the large scale atmospheric circulation.

These results suggest that an adequate representation of the seasonal cycle is important for modeling the extent of the tropics, the global mean energy budget and the magnitude of the mid-latitude atmospheric energy transport and its effect on the jets. The observed seasonal migration of the ITCZ is comparable to that of the 12 or 24 m mixed layer depth simulation (see Donohoe et al. 2013, Fig. 8). Similarly, the strength of the annual mean Hadley cell and meridional structure of the planetary albedo and precipitation in the observed climate system is comparable to that of the 12 m slab ocean aquaplanet simulation. In comparison, the strength of the annual mean Hadley in the 50 m simulation is a factor of four larger than the observations (bottom panel of Fig. 5) and the annual mean precipitation and planetary albedo barely peaks in the tropics in the 2.4 m run. Clearly, the seasonal migration of the ITCZ makes an impact on mean climate in the observations and, if the magnitude of the seasonal cycle is unreasonable, the basic state climate, including the extratropical atmospheric circulation, will not be adequately represented. Thus, one should be cautious when interpreting results from climate simulations forced by annual mean (or equinoctial insolation) or seasonal slab ocean simulations with extreme mixed layer depths.

**Acknowledgments** AD was funded by the NOAA Global Change Postdoctoral Fellowship.

## References

- Andrews D, McIntyre M (1976) Planetary waves in horizontal and vertical shear: the generalized Eliassen-palm relation and the zonal mean acceleration. *J Atmos Sci* 33:2031–2048
- Chiang J, Friedman A (2012) Extratropical cooling, interhemispheric thermal gradients, and tropical climate change. *Annu Rev Earth Planet Sci* 40:383–412
- Chou M, Lee K (1996) Parameterizations for the absorption of solar radiation by water vapor and ozone. *J Atmos Sci* 53:1203–1208
- Czaja A, Marshall J (2006) The partitioning of poleward heat transport between the atmosphere and the ocean. *J Atmos Sci* 63:1498–1511

- Danabasoglu G, Gent P (2009) Equilibrium climate sensitivity: is it accurate to use a slab ocean model? *J Clim* 22:2494–2499
- Delworth TL, Broccoli AJ, Rosati A, Stouffer RJ, Balaji V, Beesley JA, Cooke WF (2006) Gfdl's cm2 global coupled climate models. part I: formulation and simulation characteristics. *J Clim* 19:643–674
- Donohoe A (2011) Radiative and dynamic controls of global scale energy fluxes. Ph.D. thesis, University of Washington, p 137
- Donohoe A, Battisti D (2012) What determines meridional heat transport in climate models? *J Clim* 25:3832–3850
- Donohoe A, Battisti D (2013) The seasonal cycle of atmospheric heating and temperature
- Donohoe A, Marshall J, Ferreira D, McGee D (2013) The relationship between ITCZ location and atmospheric heat transport across the equator: from the seasonal cycle to the last glacial maximum. *J Clim* 26(11):3597–3618
- Edmon HJ, Hoskins B, McIntyre M (1980) Eliassen-palm cross sections for the troposphere. *J Atmos Sci* 37:2600–2616
- Eliassen A, Palm E (1961) On the transfer of energy in stationary mountain waves. *Geophys Publ* 22(5):1–23
- Enderton D, Marshall J (2009) Controls on the total dynamical heat transport of the atmosphere and oceans. *J Atmos Sci* 66:1593–1611
- Fasullo JT, Trenberth KE (2008a) The annual cycle of the energy budget: part 1. Global mean and land-ocean exchanges. *J Clim* 21:2297–2312
- Fasullo JT, Trenberth KE (2008b) The annual cycle of the energy budget: part 2. Meridional structures and poleward transports. *J Clim* 21:2313–2325
- Frierson D, Hwang Y, Fuckar N, Seager R, Kang S, Donohoe A, Maroon E, Liu X, Battisti D (2013) Why does tropical rainfall peak in the northern hemisphere? The role of the oceans meridional overturning circulation. *Nature* (submitted)
- Johanson C, Fu Q (2009) Hadley cell widening: model simulations versus observations. *J Clim* 22:2713–2725
- Kang S, Held I, Frierson D, Zhao M (2008) The response of the ITCZ to extratropical thermal forcing: idealized slab-ocean experiments with a GCM. *J Clim* 21:3521–3532
- Lin SJ (2004) A “vertically lagrangian” finite-volume dynamical core for global models. *Mon Weather Rev* 132:2293–2307
- Lindzen R, Hou A (1988) Hadley circulations of zonally averaged heating centered off the equator. *J Atmos Sci* 45:2416–2427
- North GR (1975) Theory of energy-balance climate models. *J Atmos Sci* 32:2033–2043
- Rose B, Ferreira D (2013) Ocean heat transport and water vapor greenhouse in a warm equable climate: a new look at the low gradient paradox. *J Clim* (in press)
- Schneider EK (1996) A note on the annual cycle of sea surface temperature at the equator. Technical Report. Center for Ocean-Land-Atmosphere Studies, 18 p
- Stone P (1978) Constraints on dynamical transports of energy on a spherical planet. *Dyn Atmos Oceans* 2:123–139
- Stone P, Salustri G (1984) Generalization of the quasi-geostrophic Eliassen-palm flux to include eddy forcing of condensational heating. *J Atmos Sci* 41:3527–3535
- Trenberth KE, Caron JM (2001) Estimates of meridional atmosphere and ocean heat transports. *J Clim* 14:3433–3443
- Vallis GK (2006) Atmospheric and oceanic fluid dynamics. Cambridge University Press, Cambridge
- Wielicki B, Barkstrom B, Harrison E, Lee R, Smith G, Cooper J (1996) Clouds and the earth's radiant energy system (CERES): An earth observing system experiment. *Bull Am Meteorol Soc* 77:853–868